Research Article | Vol. 27, No. 20 / 30 September 2019 / Optics Express 27702
Optics EXPRESS

Analysis of electromagnetic vortex beams using modified dynamic mode decomposition in spatial angular domain

YANMING ZHANG,[1,2] MENGLIN L. N. CHEN,[1,2] AND LI JUN JIANG[1,2,*]

[1]Department of Electrical and Electronic Engineering, University of Hong Kong, Pokfulam, Hong Kong
[2]HKU Shenzhen Institute of Research and Innovation, Shenzhen 518057, China
[*]jianglj@hku.hk

Abstract: The orbital angular momentum (OAM) modes of electromagnetic (EM) beams are utilized for multiplexing in communication systems, where each OAM mode is encoded with data. The OAM index, or the so-called topological charge, identifies each OAM mode. Recently, the amplitude of OAM mode has also been used as another modulation format. Therefore, accurate extraction of not only the OAM index but also the corresponding amplitude is required. In this paper, a modified dynamic mode decomposition (DMD) algorithm is proposed to analyze the OAM modes. We show that accurate topological charges and high-resolution amplitude patterns of both single OAM mode and composite OAM modes can be obtained. This work offers an effective approach for demultiplexing OAM-carrying beams, especially when the high-resolution amplitude information is needed.

1. Introduction

Since the orbital angular momentum (OAM) in electromagnetic (EM) beams was recognized by Allen et al. [1], it has been analyzed extensively, including its generation, transmission, and detection [2–11]. The OAM-carrying beams have been applied in the detection of rotating objects, atom trapping, stimulated emission depletion microscopy [12–14] and particularly, communication systems [15]. Compared with plane waves, the OAM-carrying beams have helical wavefronts, resulting from an additional phase term, $e^{jl\phi}$ (l is the topological charge and ϕ is the azimuthal angle) in the field equation. Unlike the spin angular momentum (SAM) that only offers two orthogonal polarization states, the OAM can take unlimited number of values so that it can offer infinite eigenstates. Moreover, the amplitude of each orthogonal OAM mode can also be modulated as a carrier of information [16,17]. Nevertheless, it is worth noting that the number of communication channels is limited by the size of the transmitter aperture, which applies for any type of multiplexing [18]. But OAM multiplexing still has its advantages, such as the simplicity due to the discard of signal processing process.

For OAM detection and demultiplexing, Fourier transform (FT) based mode decomposition was first proposed and has been widely employed [19–21]. In this method, the topological charge of EM field at one specific radial position is extracted. However, this method is limited by the uncertainty principle [22], which means the information along the angular direction is lost. Afterwards, empirical mode decomposition (EMD) method was proposed [23]. By using this method, local topological charges of superposed OAM modes along the angular direction are obtained. However, for both the FT and EMD methods, a radial position should be selected first and the topological charge and field amplitude of each OAM mode are calculated at this specific radial position. When the superposed OAM modes have different waists, which is the usual case, their amplitudes at one radial position will be misleading. Therefore, it is necessary to develop an analysis tool to obtain the topological charges as well as the amplitude patterns

#370365 https://doi.org/10.1364/OE.27.027702
Journal © 2019 Received 27 Jun 2019; revised 24 Aug 2019; accepted 2 Sep 2019; published 17 Sep 2019

Optics EXPRESS

along the radial direction for superposed OAM-carrying beams. In this paper, we introduce the dynamic mode decomposition (DMD) to address this challenge. The DMD was first proposed in hydrodynamics to compute the oscillation frequency and decay/growth rate of a spatial-temporal signal [24]. Since then, it has been applied in many fields, such as discovering governing equation in nonlinear system, global power system, chaos analysis and the spread of infections [25–28]. Interestingly, there is an analogy between the time oscillation term, $e^{j\omega t}$ and the phase term of an OAM mode, $e^{jl\phi}$. So, when ω can be obtained by providing the time series of data through DMD, we should be able to obtain the OAM index l, by providing the azimuthal series of field.

In this paper, we demonstrate a modified DMD algorithm to analyze the superposed OAM-carrying beams. By replacing the information in temporal domain with the EM fields in angular domain, we can compute the topological charge l, instead of the angular frequency ω. Then, the amplitude pattern of each decomposed OAM mode along the radial direction can be constructed, which is similar to the extraction of the time dynamic modes. The radiated EM fields from uniform circular arrays (UCAs) are analyzed. According to our searches, this is the first effort in using the DMD approach for OAM mode analysis. Our contribution lies in several aspects. Firstly, unlike other sort method, such as FT and EMD, our data-driven method does not require integration calculation and iterative computation so that it can sort the superposed OAM modes very efficiently. Besides, our data-driven method requires less measured or simulated data than the machine learning method, because there is no need for the training process. Secondly, our method considers the spatial-angular correlation. It can extract both the topological charges and corresponding amplitudes simultaneously. It helps us understand the spatial-angular OAM-carrying beams. Finally, we prove that our approach could also be used to sort superposed OAM-carrying beams with partial angular receiving aperture. Hence, the proposed method could be a better tool for analyzing OAM modes.

2. Theoretical principle

The electric field of an OAM-carrying beam can be expressed by

$$E(r,\phi) = \sum_{i=1}^{n} A_i(r) e^{jl_i\phi} \tag{1}$$

where r is the radial position, ϕ is the azimuthal position, l_i is the topological charge, and $A_i(r)$ is the amplitude which is solely dependent on r.

The conventional DMD method deals with a spatial-temporal correlated signal. Here, the temporal domain ($e^{j\omega t}$) is transformed into the angular domain ($e^{jl_i\phi}$). And we consider the amplitude term, $A_i(r)$ as the spatial domain. Therefore, the OAM-carrying beams become spatial-angular correlated signals. To be specific, the electric field of an OAM-carrying beam forms an input signal and is arranged in the form of an azimuthal snapshot sequence:

$$\boldsymbol{\Psi} = [\boldsymbol{\psi}(r,\phi_0), \boldsymbol{\psi}(r,\phi_1) \cdots\cdots \boldsymbol{\psi}(r,\phi_{n-1})]^{\top} \tag{2}$$

$$\boldsymbol{\Psi}' = [\boldsymbol{\psi}(r,\phi_1), \boldsymbol{\psi}(r,\phi_2) \cdots\cdots \boldsymbol{\psi}(r,\phi_n)]^{\top} \tag{3}$$

Here, $\boldsymbol{\psi}(r,\phi_i)$ are column vectors and each column element corresponds to the data at a specific r position. The snapshots with phase interval $\Delta\phi$ are assumed to be related by a mapping matrix $\boldsymbol{F}$, i.e. $\boldsymbol{\psi}(r,\phi_{i+1}) = \boldsymbol{F}\boldsymbol{\psi}(r,\phi_i)$. Rewriting it in matrix form, we have

$$\boldsymbol{\Psi}' = \boldsymbol{A}\boldsymbol{\Psi} \tag{4}$$

The output of DMD is the leading eigenvalues and eigenvectors of matrix $\boldsymbol{A}$, which determines the dynamic behavior of the system. We employ the singular value decomposition (SVD)-based approach to implement DMD.

Optics EXPRESS

Firstly, the SVD of $\boldsymbol{\Psi}$ is written as

$$\boldsymbol{\Psi} = \boldsymbol{U}\boldsymbol{\Sigma}\boldsymbol{V}^{*} \tag{5}$$

where $*$ means the conjugate transpose. Substituting Eq. (5) into Eq. (4), one can obtain

$$\boldsymbol{A} = \boldsymbol{\Psi}^{'}\boldsymbol{V}\boldsymbol{\Sigma}^{-1}\boldsymbol{U}^{*} \tag{6}$$

To project $\boldsymbol{\Psi}^{'}$ onto proper orthogonal decomposition (POD) modes for efficient computation, we do a similarity transform by using matrix $\boldsymbol{U}$:

$$\widetilde{\boldsymbol{A}} = \boldsymbol{U}^{*}\boldsymbol{A}\boldsymbol{U} \tag{7}$$

Combining Eq. (4) and Eq. (7), we have

$$\widetilde{\boldsymbol{\Psi}}^{'} = \widetilde{\boldsymbol{A}}\widetilde{\boldsymbol{\Psi}} \tag{8}$$

where $\widetilde{\boldsymbol{\Psi}} = \boldsymbol{U}^{*}\boldsymbol{\Psi}$. $\widetilde{\boldsymbol{\Psi}}$ is the low-dimensional representation of the linear system on the POD basis and $\widetilde{\boldsymbol{A}}$ captures the modes (the dynamic OAM system) in this low-dimensional system. The eigenvalue equation for this system can be written as the matrix multiplication

$$\widetilde{\boldsymbol{A}}\boldsymbol{W} = \boldsymbol{W}\boldsymbol{\Lambda} \tag{9}$$

where $\boldsymbol{W}$ is a square matrix of order m. The columns of $\boldsymbol{W}$ are the eigenvectors and $\boldsymbol{\Lambda}$ is a diagonal matrix containing the corresponding eigenvalues $\lambda_k, k = 1, 2 \cdots m$.

Then, the dynamic modes in the original OAM system is written as

$$\boldsymbol{S} = \boldsymbol{\Psi}^{'}\boldsymbol{V}\boldsymbol{\Sigma}^{-1}\boldsymbol{W} \tag{10}$$

Finally, the input signal at a snapshot, i.e. the electric field of the beam at an azimuthal position, is decomposed as

$$\boldsymbol{\psi}(r, \phi_i) = \sum_{k=1}^{m} \boldsymbol{s}_k e^{\omega_k \phi_i} b_k = \sum_{k=1}^{m} \boldsymbol{s}_k e^{\omega_k^r \phi_i} e^{j\omega_k^i \phi_i} b_k \tag{11}$$

where $\boldsymbol{s}_k$ is the k^{th} column of the matrix $\boldsymbol{S}$, $\omega_k = \omega_k^r + j\omega_k^i = \ln(\lambda_k)/\Delta\phi$, and b_k is the amplitude weight of the k^{th} eigenmode. The physical meaning of Eq. (11) is straightforward. The OAM-carrying beam is decomposed into m modes. $e^{\omega_k \phi_i}$ relates to the phase term $e^{jl\phi}$. So, the mode with non-zero real part of ω_k corresponds to an evanescent wave that can be abandoned. Only the modes with only imaginary part of ω_k are the OAM modes with topological charges equal to ω_k^i. $\boldsymbol{s}_k b_k$ is the corresponding amplitude distribution along the radial direction.

3. Simulation results

We first analyze a Laguerre-Gaussian beam described by Eq. (1). For the LG_{l0} mode, near its beam waist, its amplitude can be expressed as

$$A(r) = r^{l} e^{-r^2/w^2} \tag{12}$$

where w is beam waist. We choose $l = 3$ and the real part of its electric field is plotted in Fig. 1(a). To apply the modified DMD, the field is discretized along the azimuthal and radial directions into 200×200 pixels. Only one eigenmode with zero ω_k^r is found. Figure 1(b) shows the extracted mode amplitude together with the analytical amplitude along the radial direction. They show a good agreement. Because this beam is generated by the analytical formula, it has high purity without noise. The real part of ω_k should be exactly zero. In Fig. 1(c), we examine the real part of $e^{\omega_k \phi_i}$ along the azimuthal direction. We can see that this mode is undamped, just as the

Optics EXPRESS

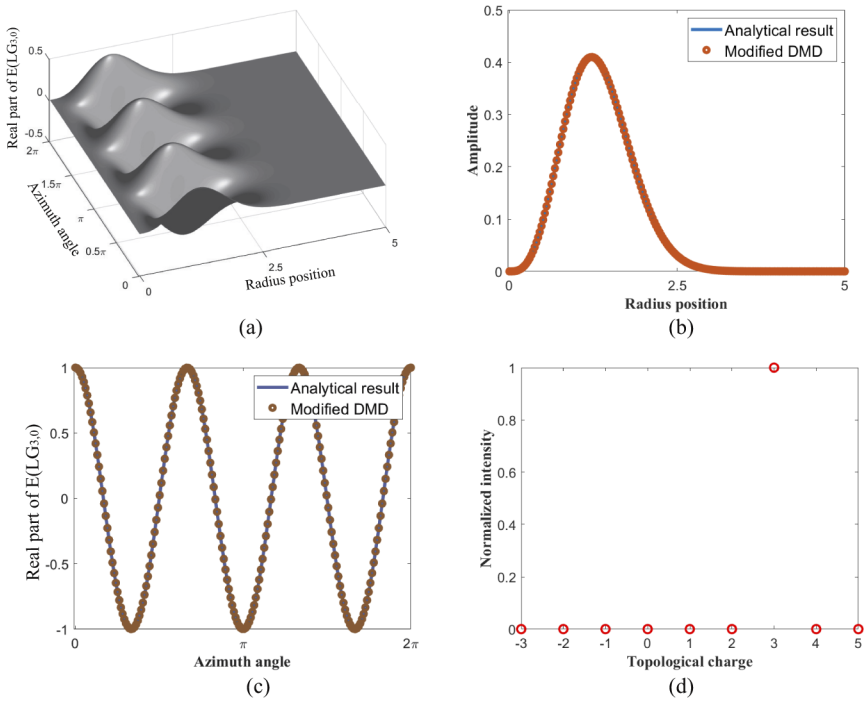

Fig. 1. (a) The real part of the electric field of the $LG_{3,0}$ beam described by Eq. (1). (b) The comparison between the analytical and extracted amplitudes of the $LG_{3,0}$ beam through the modified DMD. (c) The comparison between the real-space distribution of the analytical and extracted electric fields along the azimuthal direction. (d) The calculated topological charge by FT.

$LG_{3,0}$ mode, which implies a zero ω_k^r. In addition, the topological charge of each OAM mode represents the oscillation frequency in angular domain. For the $LG_{3,0}$ mode, there are three complete periods in the range of 2π along the azimuthal direction, so the extracted ω_k^i is equal to 3 exactly. For comparison, the topological charge calculated based on FT is plotted in Fig. 1(d). The correct result is obtained, but clearly, the information along the azimuthal direction is lost.

For mixed Laguerre-Gaussian beams ($l_1 = 1, l_2 = 2, l_3 = 3$), Fig. 2(a) shows the composite electric-field distribution, calculated by Eq. (1). Through the modified DMD, three OAM modes are extracted and presented in Fig. 2(b), and they are consistent with the analytical field distribution. Meanwhile, the angular patterns that include the information of topological charge of each OAM beam are also drawn in Fig. 2(c). It is found that the extracted topological charge of each OAM mode also agrees well with the generated raw Laguerre-Gaussian beams. Besides, the result calculated by FT is also shown in Fig. 2(d). The radial position for the extraction is at 1 m, where the intensities of the three OAM modes are equal. We can see that the FT can accurately extract the OAM-mode orders and weights. However, it is hard to apply the FT in analyzing the radial distributions of the modes, while the modified DMD can extract the exact amplitude distributions of different OAM modes in high resolution (Fig. 2(b)).

The fractional electromagnetic vortex (FEV) breaks the orthogonality of the OAM modes, so it is difficult to accurately measure the fractional topological charges by using FT-based methods. Interestingly, the DMD extracts the characteristic modes from the data directly without providing the basis for mapping. Therefore, our proposed modified DMD can be perfectly applied in the analysis of OAM modes with fractional topological charges. To demonstrate its validity, we consider mixed Laguerre-Gaussian beams with $l_1 = 1.5, l_2 = 2.5, l_3 = 3.5$. Figure 3(a) shows

Optics EXPRESS

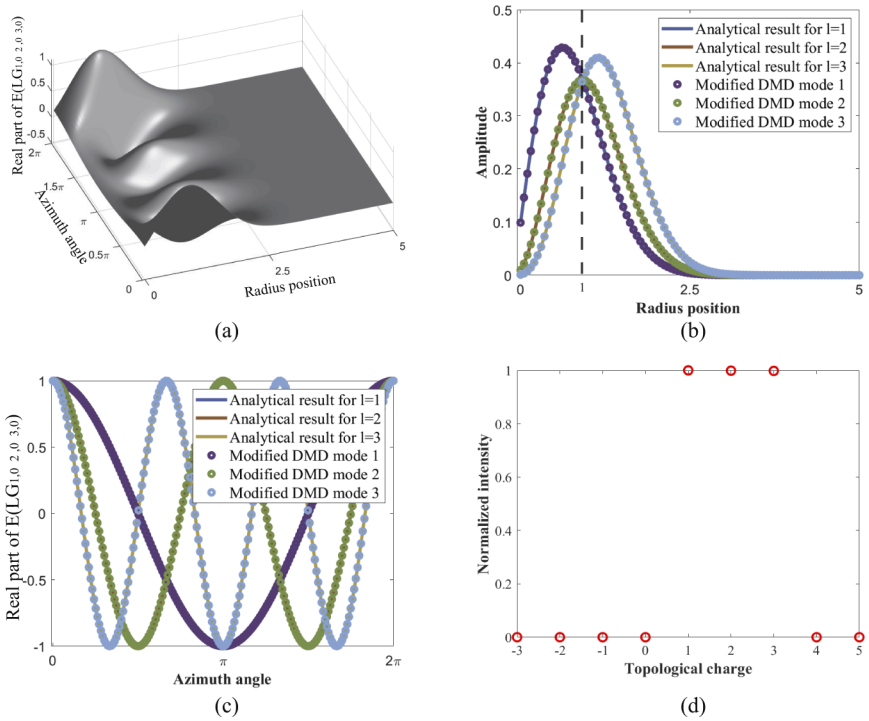

Fig. 2. (a) The real part of the electric field of the mixed Laguerre-Gaussian beams with $l_1 = 1, l_2 = 2, l_3 = 3$ described by Eq. (1). (b) The comparison between the analytical and extracted amplitudes of the mixed beams through the modified DMD. (c) The comparison between the real-space distribution of the analytical and extracted electric fields along the azimuthal direction. (d) The calculated topological charge by FT.

the composite electric-field distribution, obtained from Eq. (1). Through the modified DMD, three OAM modes are extracted. As shown in Fig. 3(b), their radial distributions agree well with the analytical results. Meanwhile, the angular patterns that include the information of topological charge of each OAM beam are shown in Fig. 3(c), which are also consistent with the raw Laguerre-Gaussian beams. The result calculated by FT is also presented in Fig. 3(d). The interval of the topological charges for the basis in the FT is 0.1. The radial position for the extraction is at 1 m. Clearly, due to the orthogonality of the projecting modes are broken, although OAM modes with $l_1 = 1.5, l_2 = 2.5, l_3 = 3.5$ appear with the same intensity, fake OAM modes also show up. Therefore, while FT limits its application in analyzing the modes with orthogonality, the proposed modified DMD method can be used for the analysis of OAM beams with both fractional and integer topological charges.

To further validate the practical significance of the modified DMD method, two cases where the OAM-carrying beams are generated by uniform circular arrays (UCAs) are considered [29,30].

A UCA has its array elements uniformly distributed along the circumference of a circle. It was firstly utilized to generate OAM-carrying beams in low-frequency radio regime [29], and then it was employed widely in the microwave band [30]. The configurations of two UCAs are shown in Fig. 4. In Fig. 4(a), N electrical dipole antennas are located equidistantly around the perimeter of a circle and the phase difference between adjacent antennas is $\Delta\phi = 2\pi l/N$, where l refers to the topological charge of designed OAM mode. The system with two UCAs in Fig. 4(b) generates superposed vortex beams. Each UCA radiates an OAM-carrying beam of order l.

Optics EXPRESS

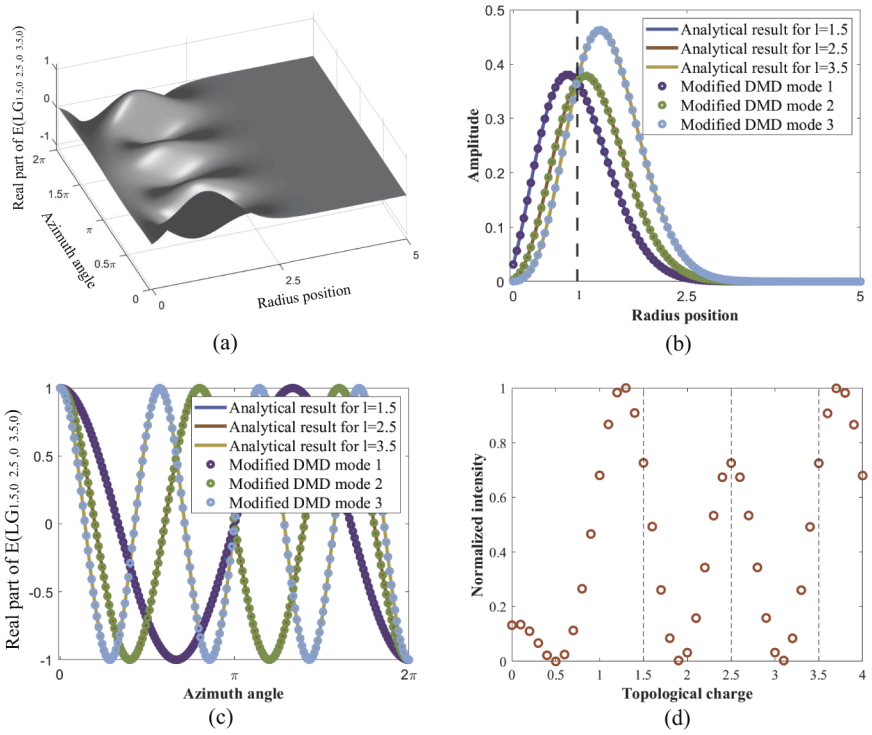

Fig. 3. (a) The real part of the electric field of the mixed Laguerre-Gaussian beams with $l_1 = 1.5, l_2 = 2.5, l_3 = 3.5$ described by Eq. (1). (b) The comparison between the analytical and extracted amplitudes of the mixed beams through the modified DMD. (c) The comparison between the real-space distribution of the analytical and extracted electric fields along the azimuthal direction. (d) The calculated topological charge by FT.

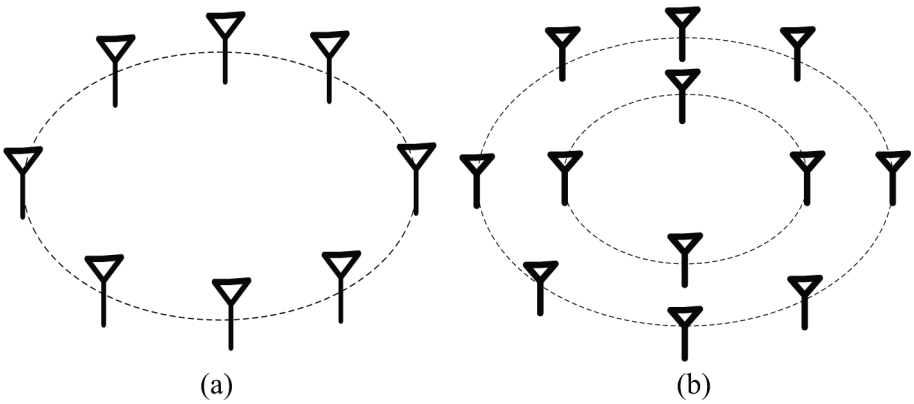

Fig. 4. Configurations of the UCAs for OAM generation. (a) UCA for single OAM-carrying beam generation. N electrically short dipoles that are equidistantly spaced along the perimeter of a circle. In this case, UCA has 16 electrical dipoles and the phase difference between adjacent antennas is $\pi/4$. (b) Two UCAs for two mixed OAM-carrying beams generation. In this case, the inner and outer UCA both have 16 electrical dipoles and the phase differences between adjacent antennas are $\pi/8$ and $3\pi/8$ respectively.

Optics EXPRESS

Firstly, we use the UCA in Fig. 4(a) with $l = 2$. Here, the radius of the UCA, $R = 60$ mm, $N = 16$, and $\Delta\phi = 2\pi l/N = \pi/4$. Full-wave simulation is done in CST Microwave Studio. Figures 5(a) and 5(b) show the simulated amplitude and phase distributions of E_z on a transverse plane $3R$ away from the UCA. The observation window is $8R \times 8R$. The OAM mode with $l = 2$ is observed. The spatial resolution depends on the sampling resolution (in this case, 1000 points are collected in x and y direction respectively so the resolution is 0.48 mm in cartesian coordinates). To fulfill the form of an azimuthal snapshot sequence (see Eq. (2) and Eq. (3)), the cartesian coordinates are converted to polar coordinates. Figure 5(c) shows the extracted mode amplitude. Clearly, we find two dips along the radial direction. The one at the origin corresponds to the singularity point of an OAM mode as in Fig. 5(a). The other dip corresponds to the sidelobe in the radiation pattern, which is consistent with the small amplitude around the blue annular area in Fig. 5(a). Meanwhile, the angular distribution of the extracted real-space electric field is drawn in Fig. 5(d), which implies a topological charge of 2. It should be noted that the proposed method deals with the acquired field information, which can be considered as the co-polarized field component. The co-polarized field component can be linearly polarized or circularly polarized, depending on the system. That is to say, the polarization should be known in prior and the proposed algorithm itself is unable to distinguish the polarization states.

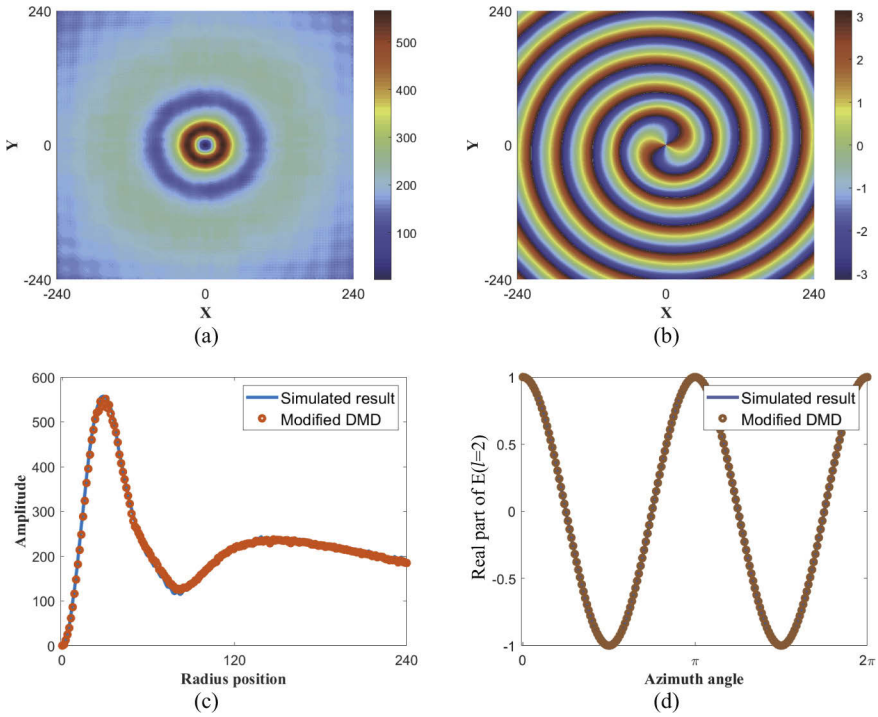

Fig. 5. Analysis of the single OAM-carrying beam. The simulated (a) amplitude and (b) phase of the OAM beam at a transverse plane $3R$ above the UCA. The extracted (c) mode amplitude along the radial direction and (d) real-space distribution of the electric field along the angular direction. Parameters are: simulation frequency $f = 10$ GHz, $N = 16$ and $l = 2$.

Then, the mixed OAM-carrying beams are generated by the UCAs shown in Fig. 4(b). The UCA on each circle has $N = 16$ electrically short dipoles. The inner UCA has a phase step of $\Delta\phi_1 = 2\pi l_1/N = \pi/8$, $l_1 = 1$ and the radius $R_1 = 15$ mm. As for the outer UCA, $\Delta\phi_2 = 2\pi l_2/N = 3\pi/8$, $l_2 = 3$, and radius $R_2 = 60$ mm. The observation window is $2R_2 \times 2R_2$, lying on the transverse plane R_2 away from the UCAs. Figure 6(a) shows the simulated amplitude

Optics EXPRESS

distribution, and Fig. 6(b) shows the phase pattern. The field data within a circular area with the radius of 50 mm is used as the input signal. Figure 6(c) shows the radial distribution of the decomposed mode amplitudes. By keeping only the inner or the outer UCA, we obtain the amplitude distribution of the simulated $l = 1$ or $l = 3$ mode and compare it with the result in Fig. 6(c). They show a good agreement with each other. Meanwhile, the topological charge of each OAM mode is accurately extracted, i.e. 1 and 3, which can also be read from the results in Fig. 6(d).

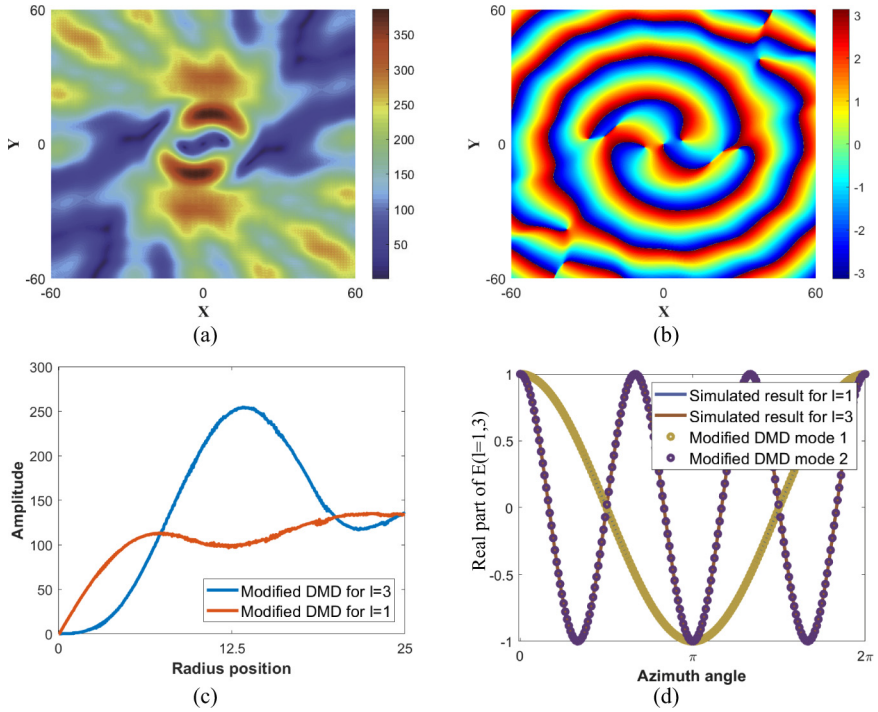

Fig. 6. Analysis of the mixed OAM-carrying beams. The simulated (a) amplitude and (b) phase of the OAM beams at a transverse plane $3R_2$ above the UCAs. The extracted (c) mode amplitudes along the radial direction and (d) real-space distributions of the electric field along the angular direction. Parameters are: simulation frequency $f = 10$ GHz. For the inner UCA, $N = 16$, and $l_1 = 1$; for the outer UCA, $N = 16$, and $l_2 = 3$.

In addition, because of the divergence of OAM beams, it is difficult to receive the whole beam aperture after long distance transmission. Our algorithm can be adapted to sort superposed OAM-carrying beams with partial angular receiving aperture. To demonstrate the partial angular aperture receiving scheme, the fields within an angular aperture from 0 to π in Figs. 6(a) and 6(b) are used as the input of our modified DMD. Figure 7(a) shows the radial distribution of the decomposed mode amplitudes. It is found that the amplitudes extracted from the partial angular aperture show the consistency with the results extracted from the whole beam (see Figs. 6(c) and 6(d)). Meanwhile, the topological charges are verfied to be 1 and 3 from the field distribution along the partial angular coordinate in Fig. 7(b).

It can be seen that this method can be conveniently employed in radio regime, since both the intensity and phase distributions of radio waves are easily accessible. However, it is rather challenging to apply the method in optical regime because the phase information is hardly obtainable. Additionally, in the real experiments, OAM-carrying beams are distorted

Optics EXPRESS

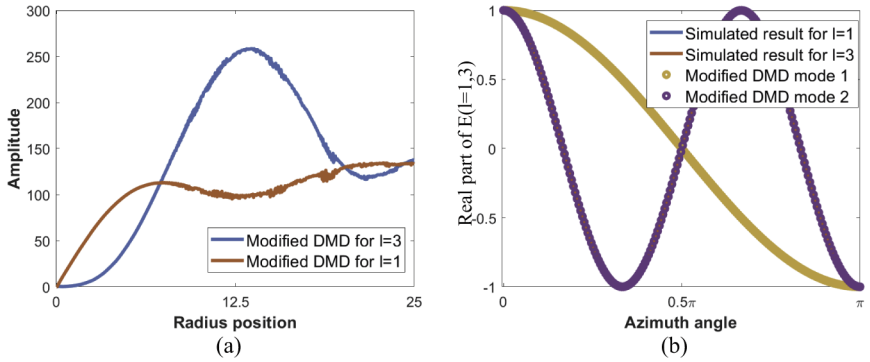

Fig. 7. Analysis of the mixed OAM-carrying beams with partial angular receiving aperture (0-π). The extracted (a) mode amplitudes along the radial direction and (b) real-space distributions of the electric field along the angular direction.

at propagation. Several advanced methods, such as the FT-based method [31] and scattering-matrix-assisted retrieval method [32] have been developed to extract the OAM modes in noisy environment. For the modified DMD method, the distortion in the input signal which depends on the amplitude and phase distributions of the electric field will perturb the mapping matrix, in both the partial and whole angular receiving cases. The matrix perturbation theory could be adopted in the modified DMD to denoise signals in the further.

4. Conclusion

In summary, we demonstrated a modified DMD approach to extract and sort the OAM modes of EM vortex beams. The modified DMD method deals with the input EM field as a spatial-angular correlated signal and decomposes it into eigenstates with different topological charges. Therefore, each eigenstate corresponds to an OAM mode and its amplitude along the radial direction can be obtained. We demonstrated the validity of the proposed approach in analyzing superposed OAM modes with not only whole receiving aperture, but also partial receiving aperture. Compared with the FT and EMD method, the modified DMD method can extract the topological charges and the amplitudes with high resolution simultaneously. It provides a practical and powerful analysis tool for the OAM demultiplexing in communication systems, especially for amplitude modulation systems.

Funding

National Natural Science Foundation of China (61271158); University of Hong Kong (201711159228); Research Grants Council, University Grants Committee (17209918); Asian Office of Aerospace Research and Development (FA2386-17-1-0010).

References

1. L. Allen, M. W. Beijersbergen, R. J. C. Spreeuw, and J. P. Woerdman, "Orbital angular momentum of light and the transformation of laguerre-gaussian laser modes," Phys. Rev. A **45**(11), 8185–8189 (1992).
2. G. Parisi, E. Mari, F. Spinello, F. Romanato, and F. Tamburini, "Manipulating intensity and phase distribution of composite laguerre-gaussian beams," Opt. Express **22**(14), 17135–17146 (2014).
3. M. L. Chen, L. J. Jiang, and E. Wei, "Ultrathin complementary metasurface for orbital angular momentum generation at microwave frequencies," IEEE Trans. Antennas Propag. **65**(1), 396–400 (2017).
4. M. L. Chen, L. J. Jiang, and W. E. Sha, "Artificial perfect electric conductor-perfect magnetic conductor anisotropic metasurface for generating orbital angular momentum of microwave with nearly perfect conversion efficiency," J. Appl. Phys. **119**(6), 064506 (2016).
5. M. L. N. Chen, L. J. Jiang, and W. E. I. Sha, "Generation of orbital angular momentum by a point defect in photonic crystals," Phys. Rev. A **10**(1), 014034 (2018).

Optics EXPRESS

6. X. Y. Z. Xiong, A. Al-Jarro, L. J. Jiang, N. C. Panoiu, and W. E. I. Sha, "Mixing of spin and orbital angular momenta via second-harmonic generation in plasmonic and dielectric chiral nanostructures," Phys. Rev. B **95**(16), 165432 (2017).
7. H. Shi, L. Wang, X. Chen, A. Zhang, and Z. Xu, "Generation of a microwave beam with both orbital and spin angular momenta using a transparent metasurface," J. Appl. Phys. **126**(6), 063108 (2019).
8. H. Shi, L. Wang, G. Peng, X. Chen, J. Li, S. Zhu, A. Zhang, and Z. Xu, "Generation of multiple modes microwave vortex beams using active metasurface," IEEE Antennas Wirel. Propag. Lett. **18**(1), 59–63 (2019).
9. G. C. G. Berkhout, M. P. J. Lavery, J. Courtial, M. W. Beijersbergen, and M. J. Padgett, "Efficient sorting of orbital angular momentum states of light," Phys. Rev. Lett. **105**(15), 153601 (2010).
10. V. A. Soifer and M. A. Golub, Laser Beam Mode Selection by Computer Generated Holograms (CRC Press, 1994).
11. C. Schulze, A. Dudley, D. Flamm, M. Duparré, and A. Forbes, "Measurement of the orbital angular momentum density of light by modal decomposition," New J. Phys. **15**(7), 073025 (2013).
12. M. P. J. Lavery, F. C. Speirits, S. M. Barnett, and M. J. Padgett, "Detection of a spinning object using light's orbital angular momentum," Science **341**(6145), 537–540 (2013).
13. T. Kuga, Y. Torii, N. Shiokawa, T. Hirano, Y. Shimizu, and H. Sasada, "Novel optical trap of atoms with a doughnut beam," Phys. Rev. Lett. **78**(25), 4713–4716 (1997).
14. T. J. Gould, S. T. Hess, and J. Bewersdorf, "Optical nanoscopy: from acquisition to analysis," Annu. Rev. Biomed. Eng. **14**(1), 231–254 (2012).
15. J. Wang, J.-Y. Yang, I. M. Fazal, N. Ahmed, Y. Yan, H. Huang, Y. Ren, Y. Yue, S. Dolinar, M. Tur, and A. E. Willner, "Terabit free-space data transmission employing orbital angular momentum multiplexing," Nat. Photonics **6**(7), 488–496 (2012).
16. S. Fu, Y. Zhai, C. Yin, H. Zhou, and C. Gao, "Mixed orbital angular momentum amplitude shift keying through a single hologram," OSA Continuum **1**(2), 295–308 (2018).
17. K. Morgan, Y. Li, W. Li, J. K. Miller, R. J. Watkins, and E. G. Johnson, "Multilevel quadrature amplitude multiplexing using coherently coupled orbital angular momentum modes," Opt. Express **26**(9), 12180–12190 (2018).
18. N. Zhao, X. Li, G. Li, and J. M. Kahn, "Capacity limits of spatially multiplexed free-space communication," Nat. Photonics **9**(12), 822–826 (2015).
19. M. Mirhosseini, M. Malik, Z. Shi, and R. W. Boyd, "Efficient separation of the orbital angular momentum eigenstates of light," Nat. Commun. **4**(1), 2781 (2013).
20. V. V. Kotlyar, S. N. Khonina, and V. A. Soifer, "Light field decomposition in angular harmonics by means of diffractive optics," J. Mod. Opt. **45**(7), 1495–1506 (1998).
21. S. Khonina, V. Kotlyar, R. Skidanov, V. Soifer, P. Laakkonen, and J. Turunen, "Gauss–laguerre modes with different indices in prescribed diffraction orders of a diffractive phase element," Opt. Commun. **175**(4-6), 301–308 (2000).
22. S. Franke-Arnold, S. M. Barnett, E. Yao, J. Leach, J. Courtial, and M. Padgett, "Uncertainty principle for angular position and angular momentum," New J. Phys. **6**, 103 (2004).
23. X. Hui, S. Zheng, W. Zhang, X. Jin, H. Chi, and X. Zhang, "Local topological charge analysis of electromagnetic vortex beam based on empirical mode decomposition," Opt. Express **24**(5), 5423–5430 (2016).
24. P. J. Schmid, "Dynamic mode decomposition of numerical and experimental data," J. Fluid Mech. **656**, 5–28 (2010).
25. S. L. Brunton, J. L. Proctor, and J. N. Kutz, "Discovering governing equations from data by sparse identification of nonlinear dynamical systems," Proc. Natl. Acad. Sci. **113**(15), 3932–3937 (2016).
26. E. Barocio, B. C. Pal, N. F. Thornhill, and A. R. Messina, "A dynamic mode decomposition framework for global power system oscillation analysis," IEEE Trans. Power. Syst. **30**(6), 2902–2912 (2015).
27. S. L. Brunton, B. W. Brunton, J. L. Proctor, E. Kaiser, and J. N. Kutz, "Chaos as an intermittently forced linear system," Nat. Commun. **8**(1), 19 (2017).
28. P. A. Eckhoff and J. L. Proctor, "Discovering dynamic patterns from infectious disease data using dynamic mode decomposition," Int. Heal. **7**(2), 139–145 (2015).
29. B. Thidé, H. Then, J. Sjöholm, K. Palmer, J. Bergman, T. D. Carozzi, Y. N. Istomin, N. H. Ibragimov, and R. Khamitova, "Utilization of photon orbital angular momentum in the low-frequency radio domain," Phys. Rev. Lett. **99**(8), 087701 (2007).
30. K. Liu, H. Liu, Y. Qin, Y. Cheng, S. Wang, X. Li, and H. Wang, "Generation of oam beams using phased array in the microwave band," IEEE Trans. Antennas Propag. **64**(9), 3850–3857 (2016).
31. L. Gong, Q. Zhao, H. Zhang, X.-Y. Hu, K. Huang, J.-M. Yang, and Y.-M. Li, "Optical orbital-angular-momentum-multiplexed data transmission under high scattering," Light: Sci. Appl. **8**(1), 27 (2019).
32. S. Khonina, S. Karpeev, and V. Paranin, "A technique for simultaneous detection of individual vortex states of laguerre–gaussian beams transmitted through an aqueous suspension of microparticles," Opt. Lasers Eng. **105**, 68–74 (2018).